6-15-2007

Dual-band negative index metamaterial: double negative at 813nm and single negative at 772nm

Uday K. Chettiar
Purdue University, uday@purdue.edu

Alexander V. Kildishev
Birck Nanotechnology Center, Purdue University, kildishev@purdue.edu

Hsiao-Kuan Yuan
Purdue University - Main Campus, hyuan@purdue.edu

Wenshan Cai
Purdue University - Main Campus, wcai@purdue.edu

Shumin Xiao
Purdue University, xiao2@purdue.edu

See next page for additional authors

Dual-band negative index metamaterial: double negative at 813 nm and single negative at 772 nm

Uday K. Chettiar, Alexander V. Kildishev, Hsiao-Kuan Yuan, Wenshan Cai, Shumin Xiao, Vladimir P. Drachev, and Vladimir M. Shalaev*

Birck Nanotechnology Center, School of Electrical and Computer Engineering, Purdue University, West Lafayette, Indiana 47907, USA

**Corresponding author: shalaev@ecn.purdue.edu*

Received January 2, 2007; revised March 30, 2007; accepted April 1, 2007; posted April 17, 2007 (Doc. ID 78578); published June 5, 2007

This work is concerned with the experimental demonstration of a dual-band negative index metamaterial. The sample is double negative (showing both a negative effective permeability and a negative effective permittivity) for linearly polarized light with a wavelength between 799 and 818 nm, and the real part of its refractive index is approximately −1.0 at 813 nm. The ratio of $-\mathrm{Re}(n)/\mathrm{Im}(n)$ is close to 1.3 at 813 nm. For an orthogonal polarization, the same sample also exhibits a negative refractive index in the visible (at 772 nm). The spectroscopic measurements of the material are in good agreement with the results obtained from a finite-element electromagnetic solver for the actual geometry of the fabricated sample at both polarizations.

OCIS codes: 160.4670, 260.5740.

The refractive index ($n=n'+in''$) is the key parameter in the interaction of light with matter. Normally n' has been considered to be positive, but the condition $n'<0$ does not violate any fundamental physical law. Negative index metamaterials (NIMs) with $n'<0$ have some remarkable properties. Typically, a NIM is an artificially engineered metal-dielectric composite that exhibits $n'<0$ within a particular wavelength range. This can be accomplished either through the strong (sufficient) condition that $\mu'<0$ and $\varepsilon'<0$, or through a more general (necessary and sufficient) condition $\varepsilon'\mu''+\mu'\varepsilon''<0$. The latter strictly implies that there cannot be $n'<0$ in a passive metamaterial with $\mu=1+0i$.

Following the above discussion, two types of NIM can be introduced. A double-negative NIM (DNNIM) is a material with simultaneously negative real parts of effective permeability and permittivity ($\varepsilon'<0$ and $\mu'<0$). A single-negative NIM (SNNIM) has a negative refractive index with either ε' or μ' (but not both) being negative. At optical wavelengths, obtaining $\varepsilon'<0$ is easy compared with obtaining $\mu'<0$, since noble metals naturally have a negative ε'.

The ratio $-n'/n''$ is often taken as a figure of merit (FOM) of NIMs, since low-loss NIMs are desired. The FOM can be rewritten as $-(|\mu|\varepsilon'+|\varepsilon|\mu')/(|\mu|\varepsilon''+|\varepsilon|\mu'')$, indicating that a DNNIM with $\mu'<0$ and $\varepsilon'<0$ is better than a SNNIM with the same $n'<0$, but with $\mu'>0$. In other words, a DNNIM will have a lower n'' when compared with a SNNIM with the same value for n'; in addition, DNNIMs can provide better impedance matching as compared to SNNIMs.

The first experimental demonstration of an NIM was given in 2001, at microwave frequencies [1]. NIMs in the optical range were studied theoretically by many researchers [2,3] before the first experimental demonstration in 2005, at 1.5 μm [4] and 2 μm [5]. In both cases a SNNIM was obtained, with FOMs of ~0.1 and 0.5, respectively. The first DNNIMs in the optical range were demonstrated at 1.4 μm with a FOM of ~3 [6] and at 1.8 μm with a FOM above 1 [7]. Most recently, negative refraction was pushed into the visible with a negative index at 780 nm [8]. This was a SNNIM with a maximum FOM of ~0.5. This Letter presents the results for a DNNIM at the shortest wavelength to date. The DNNIM has a maximum FOM of 1.3 at a wavelength of 813 nm. The same structure exhibits SNNIM behavior at 772 nm, showing negative n' at the shortest visible wavelength thus far.

It has been previously shown [5,6,9] that a subwavelength biperiodic cross grating, consisting of two perforated thin metal layers separated by a thin dielectric, is a good design prototype for NIMs. This design was used for initial sample optimization. The sample was fabricated using *e*-beam lithography followed by *e*-beam evaporation and lift-off. The structure was fabricated on a glass substrate coated with a 15 nm thick indium–tin–oxide (ITO) layer. Figure 1(a) depicts a field emission scanning electron micro-

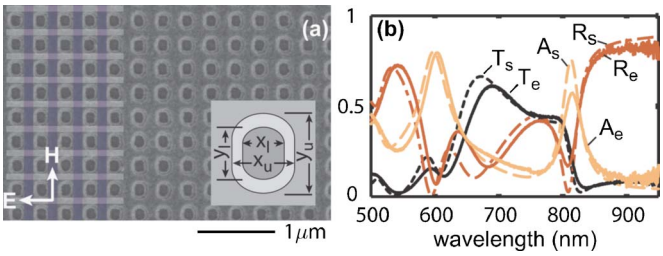

Fig. 1. (Color online) (a) Background shows the FESEM image of the NIM sample; the inset in Fig. 1(a) depicts the unit cell of the simulated structure. (b) Comparison of the experimental transmission (T_e), reflection (R_e), and absorption (A_e) spectra of the sample with simulated results (T_s, R_s, and A_s) at the primary linear polarization as shown in Fig. 1(a).

0146-9592/07/121671-3/$15.00

scope (FESEM) image of our structure, which is made of two 33 nm layers of perforated silver separated by a 38 nm layer of alumina. The lattice constant of the structure is 300 nm in both lateral directions. A 10 nm thick layer of alumina was deposited on top and beneath the structure to protect the silver from deterioration and to improve adhesion.

We first consider the double-negative regime of the structure. Figure 1(a) depicts the "primary" polarization of the incident light, creating the double-negative regime. The incident magnetic field is polarized along the set of wider parallel strips. These "magnetic strips" are schematically shown in Fig. 1(a) as darker strips on top of the FESEM background image. The magnetic strips of the upper and lower layers are coupled at the magnetic resonance; in the optimized design the magnetic resonance should be sufficiently strong, resulting in negative values for effective permeability. The other set of parallel strips, shown as lighter strips in Fig. 1(a), is aligned with the incident electric field and shows no diffraction (since the period is subwavelength). These "electric strips" behave as a diluted metal, providing a controllable broadband negative ε' [10,11]. As a result, the structure can exhibit simultaneous negative μ' and ε', demonstrating DNNIM behavior.

To validate the design, the sample was optically characterized by obtaining its transmittance and reflectance spectra using normally incident light at both the primary and secondary linear polarizations. The details of the experimental setup are described in Ref. [12]. The measured spectra for the DNNIM regime (primary polarization) are shown in Fig. 1(b). The figure compares optical measurements with the simulated data obtained from a commercial finite-element 3D full-wave electromagnetic solver (Comsol Multiphysics). The inset in Fig. 1(a) shows the unit cell of the simulated structure, where the stadium-shaped void (x_l=122 nm, x_u=218 nm, y_l=154 nm, and y_u=256 nm) follows the averaged geometry obtained in fabrication. In simulations the permittivity of silver was taken from experimental data [13], with the exception that ε'' is assumed to be three times that of bulk silver. This loss correction is made to match the experimental spectra and corresponds to additional losses in the silver due to imperfections in the metallic elements and metal–dielectric interfaces.

The experimental and simulated spectra shown in Fig. 1(b) demonstrate a good match over a broad range of measured wavelengths (from 500 to 950 nm) and include sharp resonance features: an electric resonance at ~600 nm and a magnetic resonance close to 800 nm. Simulations provide comprehensive proof of the origin of these resonances. Field maps indicate that at 815 nm the resonance is magnetic, and the electric displacement forms a loop. At 560 and 625 nm the dominant resonance is electric, with the electric displacement in both strips being almost in phase. At both polarizations, the electric and magnetic resonances are caused by the magnetic strips (strips aligned with the incident magnetic field). The electric strips have no resonant behavior.

Figure 2(a) depicts the "secondary" linear polarization, which is orthogonal to the primary polarization of the incident light. In this case, the sample changes its behavior from double negative to single negative. At the secondary polarization, the incident electric field is aligned along the set of wider parallel strips, and the magnetic field is aligned with the narrower strips. These electric strips and magnetic strips are schematically indicated in Fig. 2(a) over the FESEM image as lighter and darker strips, respectively. Note that in the secondary polarization a different set of parallel strips is coupled at the magnetic resonance.

Experimental and simulated spectra for the secondary polarization also demonstrate a good match. A selected range of prime interest (around the magnetic resonance close to 770 nm) is shown in Fig. 2(b). The unit cell and all optical constants used in the numerical simulations at the secondary polarization are identical to those used at the primary polarization. In comparison with the DNNIM regime, the magnetic strips in the single-negative case are narrower. The resonance wavelength λ_m is roughly proportional to the average width of the nanostrips; as a result, the magnetic resonance is blueshifted to 770 nm. However, the resonance is not sufficiently strong; only positive values for the effective permeability are obtained. The magnetic strips in the secondary polarization are not optimized for a strong negative magnetic response. The electric strips in the secondary polarization are too wide, resulting in a nonoptimal negative permittivity, which suppresses the magnetism even further. Hence the structure exhibits only SNNIM behavior with a positive permeability. This is confirmed by a much higher reflectance (and lower transmittance) before the resonance peak in absorbance, indicating that the structure is far from the impedance-matching condition. The structure can show dual-band magnetic responses at a linear polarization of 45° with respect to the strips.

Figures 1(b) and 2(b) demonstrate good agreement between our spectroscopic measurements and numerical simulations obtained over a wide wavelength range for two different linear polarizations. This is a good indication of the validity of the numerical model, which is used to retrieve the effective parameters of the equivalent homogenized layer. The effective parameters are obtained by utilizing an extension of a standard homogenization technique [14] for

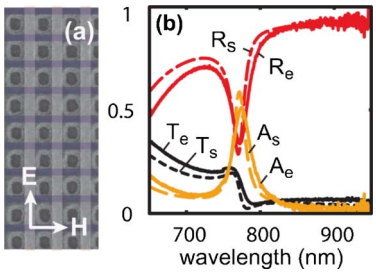

Fig. 2. (Color online) (a) Light polarization in the SNNIM regime; (b) experimental transmission (T_e), reflection (R_e), and absorption (A_e) versus the results (T_s, R_s, and A_s) obtained from numerical simulations with the polarization shown in Fig. 2(a).

a layer on a glass substrate [9]. The thickness of the equivalent homogenized layer is equal to the physical thickness of the structure including the ITO layer (i.e., 139 nm). The technique uses the complex values of reflection and transmission coefficients obtained either from the simulations or from measurements.

The retrieved results for the primary polarization are shown in Fig. 3. The real part of the refractive index (n') and the FOM ($-n'/n''$) are depicted in Fig. 3(a) (the FOM is set to zero when $n'>0$). The best FOM of 1.3 is obtained at a wavelength of 813 nm, where n' is approximately −1.0. The minimum value of the refractive index, $n'\approx-1.3$, is achieved at 820 nm, but with a lower FOM of 0.9. As indicated in Fig. 3(b), μ' is negative between 799 and 818 nm. This band is the DNNIM regime. In this range ε' varies within the range given by -1.2 ± 0.1. The strongest magnetic response ($\mu'\approx-0.7$) is obtained at a wavelength of 813 nm, where $\varepsilon'\approx-1.1$.

The magnetic resonance in periodic NIMs introduces an electric antiresonant response close to the resonant wavelength [9,11]. As presented in [15] a reversed effect should also be observed within the electric resonance band, where the magnetic antiresonance is present. In our sample, this periodicity effect can be clearly observed in Fig. 3(b), where an antiresonance of ε' coincides with the magnetic resonance at ~820 nm.

The results for the SNNIM regime obtained at the secondary polarization are shown in Fig. 4, where Fig. 4(a) depicts n' and the ratio $-n'/n''$, while Fig. 4(b) shows μ' and ε'. At this polarization, the best FOM of 0.7 is obtained at a wavelength of 772 nm, where n' is approximately −0.9. The lowest value of the refractive index ($n'\approx-1.0$) is achieved at 776 nm, but with a slightly lower FOM. Figure 4(b) shows that μ' is never negative for this polarization. Its minimum value ($\mu'\approx0.2$) is obtained at a wavelength of 769 nm along with $\varepsilon'\approx-2.0$. The SNNIM band starts at ~753 nm and ends at ~810 nm with the value of ε' decaying toward longer wavelengths from approximately −2.0 to −3.0. Similar to the DNNIM case, the typical periodicity effect is also evident in Fig. 4(b) through the antiresonant behavior of ε' at the magnetic resonance around 780 nm.

A dual-band NIM sample with a period of 300 nm in both directions was fabricated and characterized using optical measurements. Depending on the polarization of normally incident light, different spectral

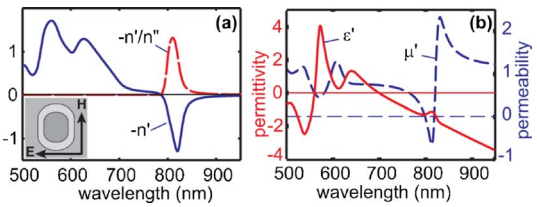

Fig. 3. (Color online) Sample in the DNNIM regime; the primary polarization of light is used in modeling as shown in the inset. (a) Real part of the effective refractive index and FOM; the FOM is set to zero if $n'>0$. (b) Real part of the effective permeability (μ') and permittivity (ε') are both negative from 799 to 818 nm.

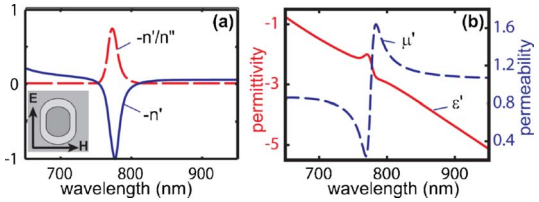

Fig. 4. (Color online) Sample in the SNNIM regime; secondary polarization of light is used in modeling as shown in the inset. (a) Real part of the effective refractive index and FOM; (b) the effective permeability (μ') is positive everywhere, and only the permittivity (ε') is negative.

behavior is demonstrated experimentally. Numerical simulations of the structure are in good agreement with optical measurements in a wide range of wavelengths for two orthogonal linear polarizations. At the primary polarization, the double-negative effective properties ($\varepsilon'<0$ and $\mu'<0$) are achieved in a 20 nm wavelength band around 810 nm; the lowest effective μ' of approximately −0.7 is observed at 813 nm along with $n'\approx-1.0$ and a FOM of ~1.3. A second wavelength band of single-negative operation is found at the orthogonal secondary polarization, where the sample exhibits NIM behavior in the visible (772 nm) with $n'\approx-0.9$ and an FOM of ~0.7.

This work was supported by U.S. Army Research Office (ARO) grant W911NF-04-1-0350 and by ARO-MURI award 50342-PH-MUR.

References

1. R. A. Shelby, D. R. Smith, and S. Schultz, Science **292**, 77 (2001).
2. V. A. Podolskiy, A. K. Sarychev, and V. M. Shalaev, J. Nonlinear Opt. Phys. Mater. **11**, 65 (2002).
3. N. C. Panoiu and R. M. Osgood, Phys. Rev. E **68**, 016611 (2003).
4. V. M. Shalaev, W. Cai, U. K. Chettiar, H.-K. Yuan, A. K. Sarychev, V. P. Drachev, and A. V. Kildishev, Opt. Lett. **30**, 3356 (2005).
5. S. Zhang, W. Fan, N. C. Panoiu, K. J. Malloy, R. M. Osgood, and S. R. J. Brueck, Phys. Rev. Lett. **95**, 137404 (2005).
6. G. Dolling, C. Enkrich, M. Wegener, C. M. Soukoulis, and S. Linden, Opt. Lett. **31**, 1800 (2006).
7. S. Zhang, W. Fan, K. J. Malloy, S. R. J. Brueck, N. C. Panoiu, and R. M. Osgood, J. Opt. Soc. Am. B **23**, 434 (2006).
8. G. Dolling, M. Wegener, C. M. Soukoulis, and S. Linden, Opt. Lett. **32**, 53 (2007).
9. A. V. Kildishev, W. Cai, U. K. Chettiar, H.-K. Yuan, A. K. Sarychev, V. P. Drachev, and V. M. Shalaev, J. Opt. Soc. Am. B **23**, 423 (2006).
10. J. B. Pendry, A. J. Holder, W. J. Stewart, and I. Youngs, Phys. Rev. Lett. **76**, 4773 (1996).
11. U. K. Chettiar, A. V. Kildishev, T. A. Klar, and V. M. Shalaev, Opt. Express **14**, 7872 (2006).
12. H.-K. Yuan, U. K. Chettiar, W. Cai, A. V. Kildishev, A. Boltasseva, V. P. Drachev, and V. M. Shalaev, Opt. Express **15**, 1076 (2007).
13. P. B. Johnson and R. W. Christy, Phys. Rev. B **6**, 4370 (1972).
14. D. R. Smith, S. Schultz, P. Markoš, and C. M. Soukoulis, Phys. Rev. B **65**, 195104 (2002).
15. T. Koschny, P. Markoš, D. R. Smith, and C. M. Soukoulis, Phys. Rev. E **68**, 065602 (2003).